



INTERNATIONAL PLANETARY AERIAL SYSTEMS CHALLENGE



Team Name: Cosmostellar

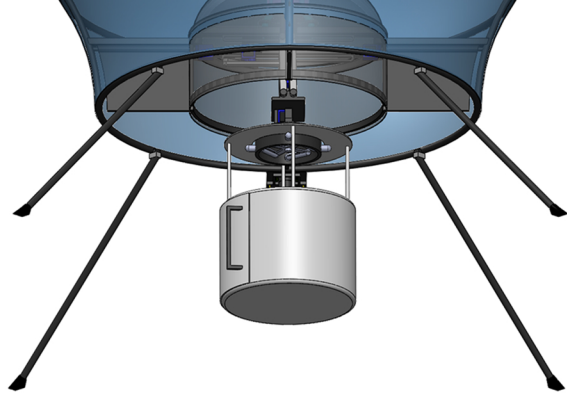
Team Lead: Punitharaj S

Lead contact: 99629 54387

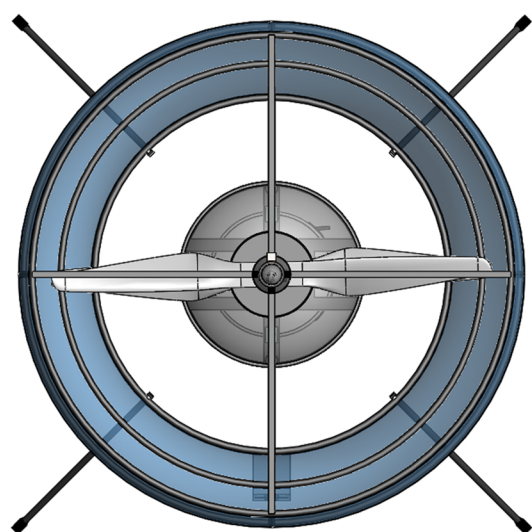
punitharaj.22meb@licet.ac.in



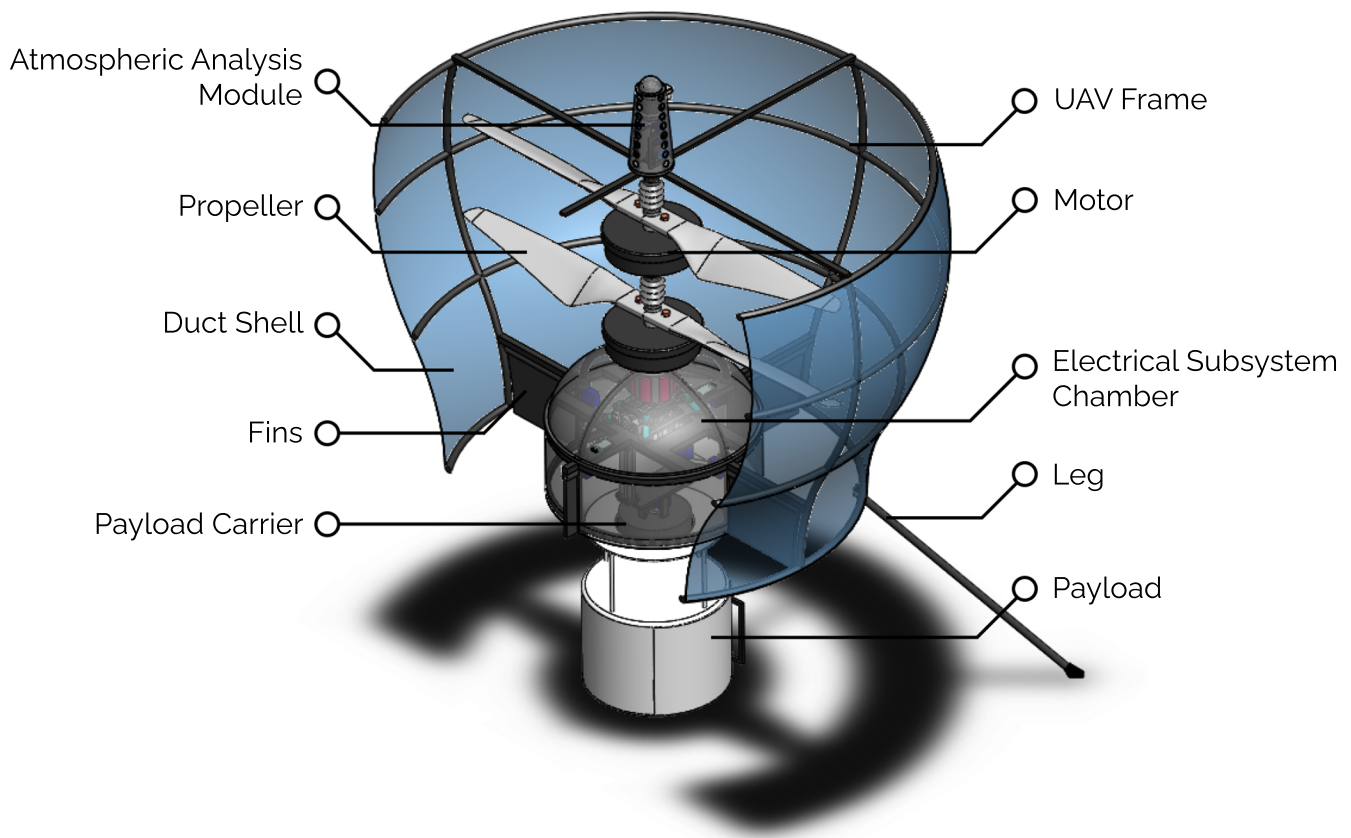
A-A Module



Vision Module



cosmostellar
stomio 1.0



Introduction:

The following pages contain a detailed engineering design report (EDR) of an Unmanned Aerial Vehicle (UAV) that is fully functional and operable in the Martian environment. The engineering constraints posed by the Martian environment are kept at the core of the UAV's design. The depth to which the UAV has been designed to comply with the martian environment is discussed in detail in the following section.

1.1 Engineering Constraints

The Martian atmosphere is complex, dynamic and challenging to fly in. One of the major reasons is its extremely lean atmosphere. Relative to the earth's atmospheric density, the highest atmospheric density of mars (found at the surface) is just 1.667% ($\sim 0.020 \text{ kg/m}^3$) [1]. This poses the constraint of weight which needs to be as minimum as possible.

The solar irradiance or the power per unit area as received by Mars from the Sun is approximately 57% lesser than what is received by Earth [1]. This results in the extremely low average temperature of the lower Martian atmosphere which is about -63°C . This means that the important electrical components must be thermally insulated and heated to their operating temperature range.

Other than that, the fluctuations in wind speed can drastically affect the thrust produced by the rotors. The dust is also an important factor as it can clog motors and other moving parts if left exposed. As the speed of sound in Mars is lesser than the speed on Earth, the rotor blade tips cannot exceed the subsonic speed range in order to avoid undesired shock wave formation. These shock waves when formed can decrease the thrust [2].

Parameter	Value
Gravity	3.721 m/s^2
Atmospheric Density	$\sim 0.020 \text{ kg/m}^3$
Atmospheric Pressure	610 Pa
Average Temperature	-63°C
Solar Irradiance	586.2 W/m^2
Wind Speed	2 - 7 m/s (summer), 5 - 10 m/s (fall), 17 - 30 m/s (dust storm)
Speed of Sound	241.4 m/s

Data as per [1] [2] [5] [6]

2. Aerodynamics Module

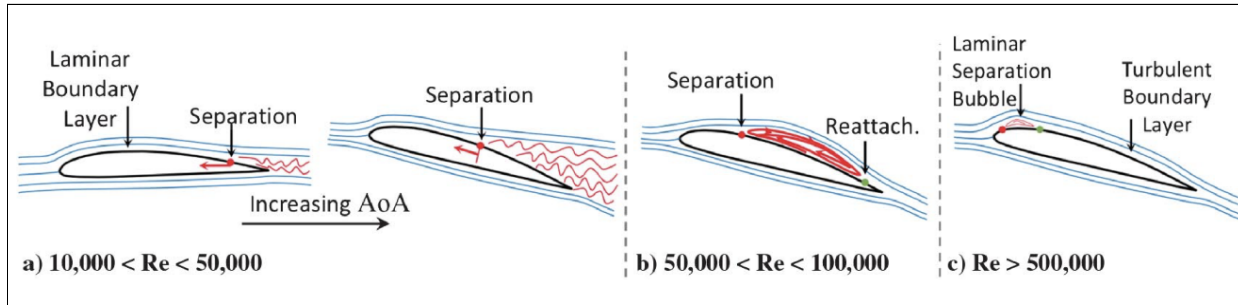
2.1 Propeller Design

The propeller needs to be designed to produce enough lift force in an atmosphere of extremely low density. The flow around the propeller is assumed to be incompressible because the velocity of the blade tips is limited to the subsonic range. Moreover, for Mars's atmospheric conditions, a low Reynold's

number and high Mach number flow is required [2]. In order to produce good thrust forces, the chord length of the blade profile has to be wide along with the overall diameter of the propeller. This design will facilitate a larger mass of fluid to be displaced downward at a minimum expenditure of energy.

2.1.1 Blade Profile

The shape of the airfoil or the blade profile is of high importance. Since we are dealing with a high Mach number flow, the blade profile has to have low thickness and large chord length. With these constraints set, for a low Reynold's number flow, separation of fluid on the upper surface of the blade is very likely to occur. This can lead to reduced lift force and an increase in pressure drag [7].



The figure is taken from [2] page 16

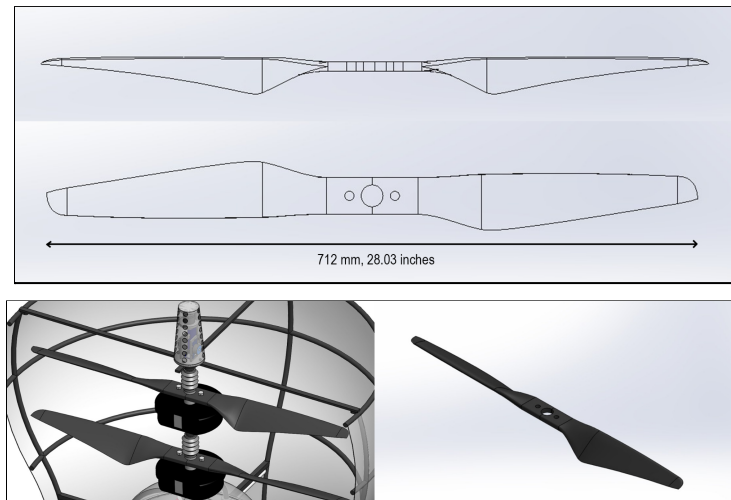
The figure above illustrates that as the angle of attack (AOA) and Reynold's number increases, the flow separation increases. Therefore, a smaller critical Reynold's number can facilitate a smoother downwash, mitigate flow separation and consequently produce greater lift force. Keeping all the constraints in mind, the airfoil that suits best for the martian atmosphere is Davis AIRFOIL (davis-il). The blade profile is shown below.



Airfoil Specification:

1. Airfoil: Davis AIRFOIL (davis-il)
2. Max thickness 11.3% at 30% chord.
3. Max camber 3.7% at 40% chord.

2.1.2 Propeller Specification



The diameter of the propeller is approximately 28 inches. One of the important characteristics of a propeller is its *geometric pitch*. To maximize the thrust and delay the stall zone of a propeller, the geometric pitch to diameter ratio should be lesser than 0.66, i.e. $P_D \leq \frac{2}{3}D$. Therefore, we have chosen the propeller pitch to be 450 mm, with a high angle of attack. Since the Martian air has extremely low density, having a high AOA will not induce as high stresses as it would if the propeller is spun in the Earth's atmosphere. The pitch-to-diameter ratio for our propeller design is given as follows:

$$\frac{P_D}{D} = 0.632$$

In order to keep the pitch-to-diameter ratio constant for all radii, the *geometric pitch angle* (β) of the propeller will vary with the distance from the axis of rotation. The geometric pitch angle can be calculated from the following formula [8]:

$$\beta = \tan^{-1}\left(\frac{P_D}{2\pi r}\right)$$

where, r is the radius at which the angle needs to be calculated. The thrust calculation of the propeller can be complicated as the AOA of the blade changes along the length. But, considering the propeller as a single disc that pushes air downwards, we can apply *simple momentum theory* [9], the thrust force can be modelled as:

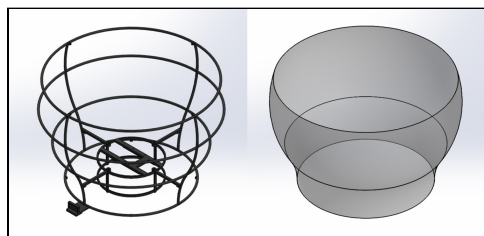
$$T = A \cdot \Delta p$$

and $\Delta p = 0.5\rho(V_e - V_i)$

where, Δp is the pressure differential relative to the inlet and outlet of flow; V_e is the exit flow velocity; V_i is the inlet flow velocity; A is the area of the propeller disc. The figure below illustrates the flow of air through a propeller.

2.2 Propeller Duct

The outer shell or the *duct* around the propeller is an unconventional design. In this section, we will discuss the reason for having the duct and how it enhances the thrust generating capacity of the propellers. **Note:** In this section, the duct is considered a single rigid body. The material and the structure of its construction is discussed in the *Mechanical* section.



2.2.1 The Design

Martian Dust:

Mars has dust storms that can cover the entire planet for a whole month. This does not happen often, but smaller dust storms are quite common [11]. Which makes it all the more important to protect the internal components of the UAV. The dust can clog the motors and the shaft bearings if left exposed too much. The duct can act as a protective shield for the UAV against large dust particles.

Nozzle Behaviour:

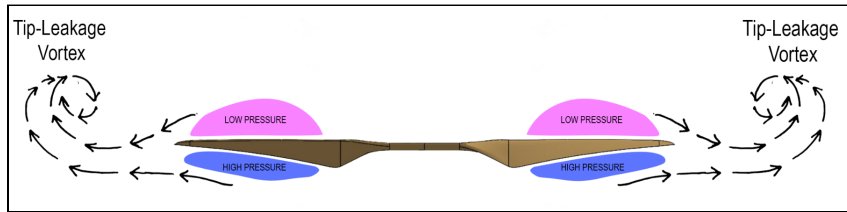
A steady flow process is a process in which the flow rate is constant and the state of the fluid at any location in the system also remains constant at any time [10]. Thus, the duct, for an incompressible flow, can be considered as a steady-state open system. The duct is designed in such a way that it follows the aerodynamics of a nozzle. Since the flow is incompressible, the mass flow rate and the pressure inside the duct-nozzle structure are constant. Hence, it follows the Steady State Energy Equation [1],

$$c_2 = \sqrt{2(h_1 - h_2) + 2g(z_1 - z_2) + c_1^2}$$

where, c_2 is accelerated outlet flow velocity; c_1 is initial velocity; $h_1 - h_2$ is the difference in enthalpy; $z_1 - z_2$ is the difference in elevation. Therefore, with accelerating nozzles, the duct increases the flow rate through the propeller, which consequently operates at a more favourable loading. The nozzle by itself produces a certain positive thrust [12].

Propeller-Tip Vortex Formation:

When studying a propeller without a duct we found out that the higher air pressure bubble underneath the blade and the low air pressure bubble over the blade surface met at the tips of the propeller. This conjunction of the two pressure bubbles occurs only in propellers due to centrifugal force. When the two pressure bubbles meet, vortex formation occurs at the tips. This means that there is a lot of wasted energy.



The tip-leakage vortex can interfere with the streamlined path in the circumferential direction and produce a negative effect on the thrust [12]. This ultimately will lead to decreased efficiency, increased noise, decreased lift, and considerable amounts of energy being taken away to form the vortices. Using the duct-like design can prevent vortex formation. A minimal amount of gap is left between the propeller and the duct (~20 mm). We get more efficiency by using less energy, which consequently reduces battery usage and increases flight time.

2.3 Fins

Aerodynamics of fins and how they facilitate direction control are explained in sections: *Flight Dynamics* and *UAV System Control*.

2.4 Simulation Results

We performed separate simulations for the propeller and the duct in ANSYS Fluent and SOLIDWORKS. The simulation results are discussed below.

Propeller Simulation Parameters	
Air Density	0.02 kg/m ³
Static Pressure	610 Pa
Air Flow Velocity	10 m/s (along Y-axis)
Gravity	3.72 m/s ²

Fluent model type	K-epsilon model	
Propeller simulation results (for one propeller)		
RPM	Thrust Generated	Torque
1800	8.89 N	1.01 Nm
2000	12.67 N	1.28 Nm
2200	14.90 N	1.51 Nm

Velocity in Stream Frame
Contour 1

Color scale: 0.000e+000 to 8.743e+001 [m s^-1]

Velocity in Stream Frame
Contour 1

Color scale: 0.000e+000 to 8.743e+001 [m s^-1]

Pressure
Contour 1

Color scale: -4.326e+003 to 2.578e+003 Pa

Velocity Streamline 1

Color scale: 0.000e+000 to 1.416e+002 [m s^-1]

Pressure Plot 1: contours

Color scale: 609.83 to 610.53 Pa

Flow Trajectories 1

Color scale: 0.964 to 9.641 m/s

The duct has been simulated using the following initial conditions:

1. Initial velocity = 4.8 m/s and 10 m/s
2. Static pressure = 610 Pa.

Initial velocity (entering the duct)	Exit velocity (leaving the duct)	Pressure Differential Δp	Theoretical Thrust $F = m_f \cdot V_e + \Delta p \cdot A_e$
4.8 m/s	9.61 m/s	0.7	19.37 N
10 m/s	19.164 m/s	0.7	38.48 N
Final Result (2000 RPM)			
Without Duct	12.67 N	With Duct	19.37 N

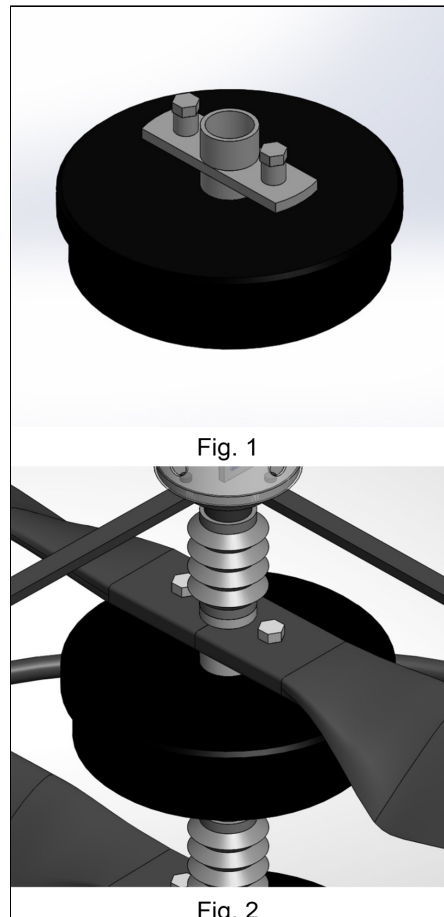
Therefore, we can justify that having a duct increases thrust, efficiency and overall lifting capacity of the UAV.

3. Electrical Subsystem

3.1 Motor Design

When it comes to high torque to weight ratio, efficiency and high speeds, the obvious choice would be a brushless DC motor (BLDC). The motor that we have designed takes most of its inspiration from GMBLF60 120-230 [13]. Our choice of motor features high efficiency and excellent controllability. Figure 1 and 2 show the motor and its mounting.

Specifications	
Rated voltage	24 Volts
Rated speed	3000
Rated torque	1.5 Nm
Peak torque	3 Nm
Rated current	15 Amps
Peak current	45 Amps
Number of poles	8
Number of phases	3
Winding connection	Star/WYE
Insulation class	Class B
Insulation resistance	100MΩ min., 500VDC



3.2 Electronic Speed Controller

The ESC is an important component as it excites the coil windings in a synchronised manner to produce a rotating magnetic field. We use a fully programmable 30A BLDC ESC with 5V, 3A BEC. It has a sturdy construction and can drive the motors continuously at 30A. Hence, it is the most suitable choice for our application.



Specifications	
Power Rating	5 Volts, 3 Amps
Output Current:	30A continuous; 40A for 10 seconds
Dimensions	55mm x 26mm x 13mm

3.2.1 ESC Protection Functions

- Abnormal Start Protection:** If the motor fails to start within 2 seconds of throttle application then ESC will cut off the output power. This situation might arise if the propellers or the motor shafts are jammed or damaged.
- Over-temperature protection:** If ESC gets heated above 1100C then it reduces the output power.
- Throttle signal loss protection:** ESC will reduce the output power to the motor if the throttle signal is lost for 1 second. If the signal is lost for further 2 seconds then it will kill the throttle and stop the motor.

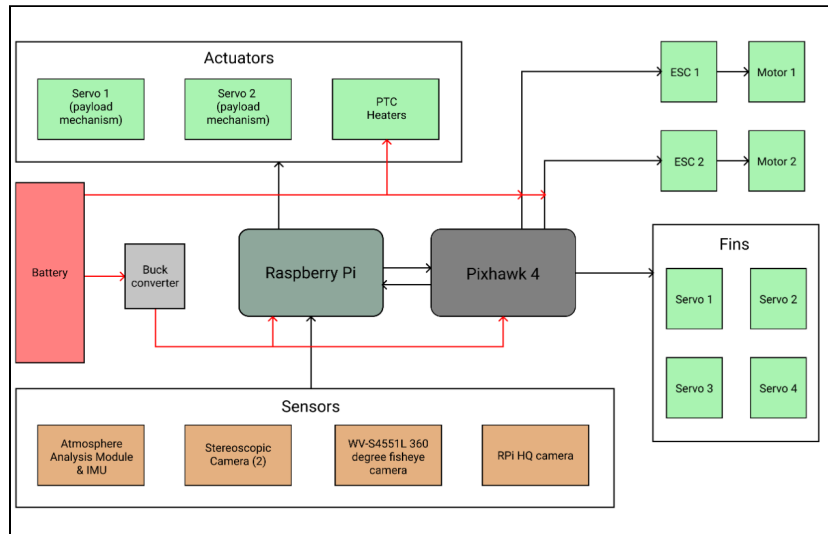
3.3 Battery or Power Source

The two major choices we had considered for choosing the right battery were Nickel-Cadmium battery and Lithium-ion battery. But Ni-Cad batteries eventually experience wear and aren't rechargeable. [14]. On the other hand, Lithium-ion batteries possess high specific energy, wide operating temperatures, and are quite reliable. Hence, they meet all the important requirements of interplanetary missions [15]. Therefore, we decided to use Lithium-Polymer batteries which possess specific energy of about 100–265 W·h/kg and an energy density of about 250–730 W·h/L [16]. The specifications of the battery used are mentioned below:

Nominal Voltage	25.6V
Nominal Capacity	10Ah
Cell Inside	LiFePO ₄ 26650 3.2V
Standard Charge Current	2A (0.2C)
Max. Charge Current	10A (1C)
Continuous Discharge Current	20A
Peak Discharge Current	40A
Fully Charged Voltage	29.2V(3.65V per cell)

Operating Temperature	Charging: 0°C ~ 45°C Discharging: -20°C ~ 55°C
Battery Management System (BMS)	BMS-L8S2005-JBD
Life Cycle	2000 times (80% of initial capacity at 0.2C rate, IEC Standard)

3.4 Circuitry and Architecture



4. Mechanical Subsystem

4.1 Materials Used

The temperatures on Mars can get extremely low. This can increase the brittleness of materials used to construct the UAV body. Moreover, we need to consider the weight constraint while choosing any material. Hence, a material which is light in weight, ductile at lower temperatures with high tensile and compressive strength is deemed suitable.

4.1.1 PTFE (Polytetrafluoroethylene)

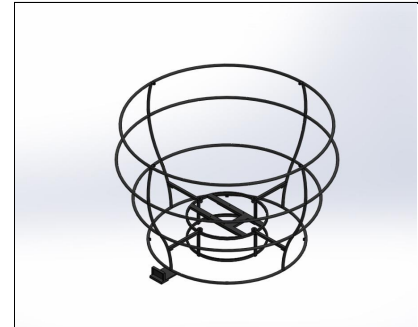
To sustain ductility at very low temperatures on Mars and also to build a reliable and lightweight UAV, PTFE is used as the outer shell for the duct. This material is proven to be ductile, light in weight and strong enough to thrive in the martian conditions. Since the outer shell is subjected to the different temperatures, pressures and thin gravity, PTFE would be a suitable material. The data in the table below was obtained from [20].

Material	Density (g/cc)	Tensile Strength (MPa)	Modulus of Elasticity (GPa)	Nature at -153 ° C
PTFE	2.2	20 - 30	0.39 - 2.25	Ductile

Aluminium alloy 7075 - T7351	2.81	505	72.0	Ductile
Nitinol 50	6.45	895 - 1100	28 -83	Ductile
Polycarbonate	1.15-1.2	61-69	2.2-2.5	Brittle
Nylon 6	1.44	40 - 100	45 - 90	Brittle

4.1.2 Carbon Fibre

The blades and the chassis of the UAV are constructed using Carbon Fibre. It can survive cold temperatures and has high tensile strength making it suitable for the propeller and chassis. The table below accounts for our decision, of using Carbon Fibre to fabricate the blades and the chassis of the UAV. The data in the table below was obtained from [19] and [21].



Material	Density (g/cm³)	Tensile Strength (MPa)	Modulus of Elasticity (GPa)
Carbon Fibre	2.00	3,530	228
Titanium	4.5	220	116
Kevlar	1.44	3,620	76
Aluminium Alloy 7075 - T7351	2.81	572	71.7

4.1.3 Carbon Fibre Composites T300

The entire body of the UAV is supported by the 4 legs, so we need a material that is sturdy. It was decided to use a material that has high compressive strength to provide a very strong base for the UAV. Carbon Fibre composite T300 is chosen for fabricating the legs of the UAV. This material seems to be a promising choice considering the varying conditions of Mars. The data in the table below was obtained from [18].

Material	Density g/cm³	Compressive Strength MPa	Modulus of Elasticity GPa
T300	1.76	1470	230
M46J	1.84	1080	436
M60J	1.93	785	588
M40J	1.77	1270	2500

T800H	1.81	1570	160
-------	------	------	-----

4.2 Thermal Module

Most electrical components are housed inside the Electrical Subsystem Chamber. This chamber requires thermal insulation and heating as certain electronic components have a particular operating temperature range. The most important component that needs to be maintained in a particular temperature range is the battery. Lithium-ion batteries perform best inside a temperature range of 10°C to +55°C. Therefore, the electrical subsystem chamber should be maintained at a minimum of 15°C at all times. In this section, we will discuss thermal insulation and heating mechanism of the chamber.

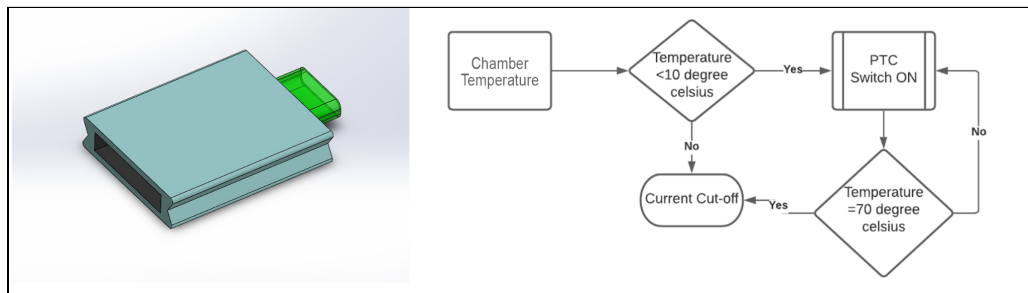
4.2.1 Thermal insulation

The outer portion of the electrical subsystem chamber is exposed to the atmosphere. Therefore heat transfer could take place due to convection. Although, the very low pressure in Mars inhibits the loss of heat due to convection, temperature inside the chamber could drop very low over time. Besides, the batteries and computation boards could experience heat dissipation due to conduction by coming in contact with the frame. Therefore it becomes doubly important to insulate the chamber.

Multi-layer insulation can be done to obtain better insulation of heat through conduction and radiation. This means that Multilayer aerogel composites are better than pure aerogel composites [22]. We chose aerogel as our primary insulating material as its thermal conductivity is almost negligible (~0.01 W/mK). Therefore, we use a thick blanket of aerogel composites covering all sides of the chamber to thermally insulate it.

4.2.2 Heating

Even after thermal insulation is done, heat can still be lost overtime. Therefore a heating mechanism needs to be implemented to not allow the temperature inside the chamber to drop below the minimum operating temperature of the battery. We use two low-power Positive Temperature Coefficient heating elements to regulate the temperature inside the chamber. The main advantage of these heaters is that it is self-regulating and can run open-loop without any external controls [23]. PTC heaters can be calibrated to operate inside a certain temperature range. Therefore, we use two 50W PTC heaters operating at 12V supply. Figure below illustrates the open-loop control of the heater.



4.3 Frame Simulation

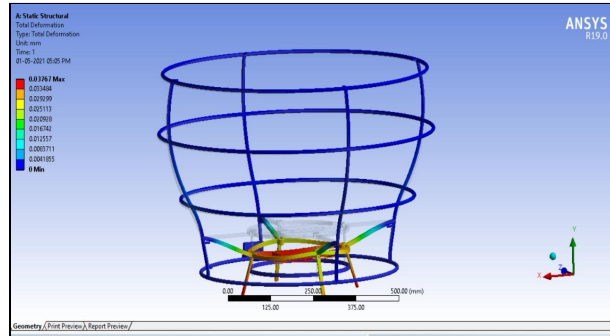
The inner chassis of the UAV is fabricated with Carbon Fibre. This module explains the structural simulation of the inner chassis in the martian conditions. The total deformation and equivalent stress are studied in the said conditions.

Plane of Axis	Young's Modulus	Poissons	Shear Modulus
---------------	-----------------	----------	---------------

	GPa	Ration	GPa
Plane of X axis	69.8	0.053	11.6
Plane of Y axis	61.1	0.383	6.80
Plane of Z axis	9.48	0.052	11.1

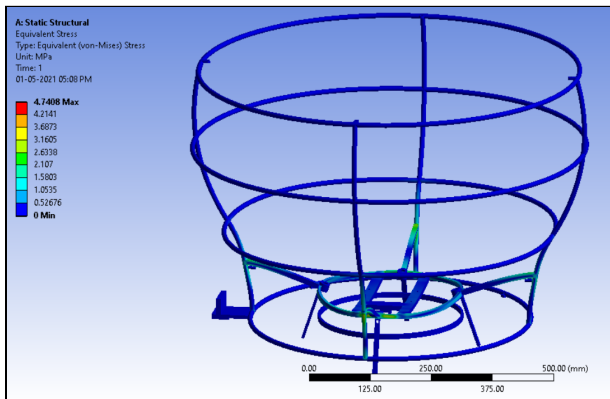
4.3.1 Total Deformation

It is evident that when load is applied on the UAV under the martian conditions, the total deformation that takes place on the inner chassis is very low. The strength of Carbon Fibre is found to be **228 GPa** and the simulated value in respect to the total deformation is **$4.0 \times 10^{-5} \text{ m}$** . This simulation proved that the material we have chosen for the inner chassis is strong enough to withstand any load applied in the varying martian conditions.



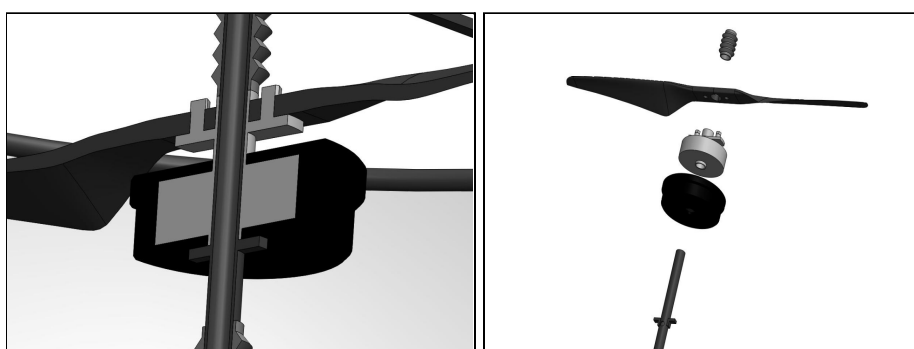
4.3.2 Von Mise's Stress

The Equivalent stress applied on the chassis is studied through the Ansys Simulation. The von mises's stress or equivalent stress is a stress limit to be maintained within the ultimate tensile strength of the material. It is seen that the lower part of the structure is subjected to the maximum stress (**3 MPa of von mises's stress**), which is less than the tensile strength (**3530 MPa**) of Carbon Fiber.



4.4 Motor Chassis Mounting

The chassis of the UAV is supported by the central support rod assembly. The propellers and motors are mounted to the support rod. The support rod is made hollow in order to accommodate wires leading up to the motors and the Atmospheric Analysis Module from the electrical subsystem chamber. The mounting design is illustrated in the following figures.



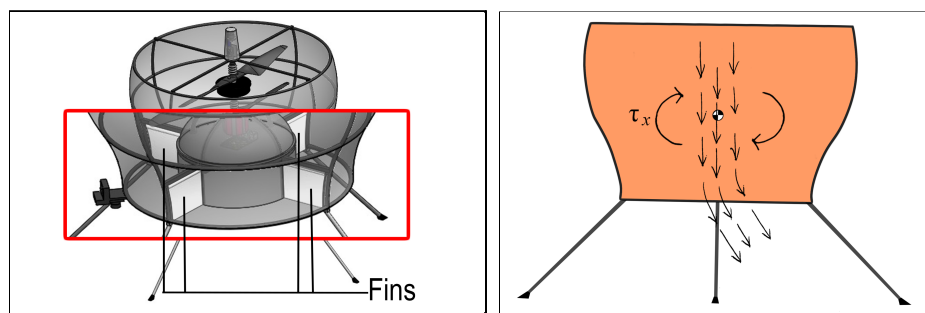
4.5 UAV Weight calculation

Component	Volume (cm ³)	Density (g/cm ³)	Mass (g)
Frame	602.8	2	1205.6
Shell	216.59	2.2	476.5
Battery + Motors	-	-	2165.0
Electrical Components, Sensors & Servo actuators	-	-	~240.0
Propellers	32.75	2	65.5
Legs	163.01	1.76	286.9
Payload Carrying Mechanism	178.18	1.76	313.6
Fins	195.39	1.76	343.9
Fasteners	-	-	100.0
Miscellaneous Parts	-	-	200.0
Total Weight			5452.9

5. Model Dynamics

5.1 Fins and Direction Control

Translational motion for the UAV in the horizontal plane (XY plane) is made possible by the fins. By controlling the angle of the fins relative to the UAV frame, a horizontal thrust vector is produced which creates a resultant torque. A set of four fins are placed along the body of the UAV as shown in the figure. Fins opposite each other are considered as pairs and each pair is controlled individually using servo motors.



Let's consider that the angle of one pair of fins is set towards the positive direction of the X-axis as shown in the figure. Part of the air moving around the fins gets deflected along the direction of fins by a phenomenon called the Coanda effect.

5.2 Thrust Division

Let's call this small space where the air experiences the Coanda effect on either side of the fins as the *Fin region*. Let the air passing through this region produce a thrust, T_f . Similarly, let the air passing outside of the fin region produce a thrust, T_n . This means the total thrust produced by the UAV when the fins are normal to the horizontal plane is, $T = T_f + T_n$

5.3 Vertical Motion

In order for the UAV to hover in mid-air, it needs to produce enough thrust force to compensate for the gravitational pull. If the rotor speed and thrust coefficient is denoted by ω and K_T respectively, then the thrust force can be described as [2],

$$T_i = K_T \omega_i^2, i = 1, 2 \dots (1)$$

For two rotors, the total thrust force is $T = T_1 + T_2$. Assuming the vertical motion is along the Z-axis, through Newton's second law, it can be described as:

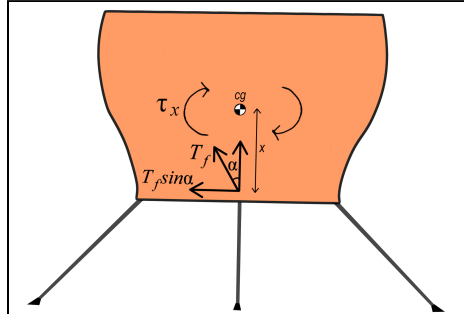
$$\ddot{Z} = \frac{T - mg}{m} \dots (2)$$

5.4 Rolling and Pitching

Consider that the UAV experiences roll about the X-axis. Therefore, the rolling moment can be modelled as,

$$\tau_x = T_f \sin\alpha \cdot x, \dots (3)$$

where α is the angle made by one pair of fins and x is the distance between the centre of gravity and fins.



Now, considering that UAV pitches about the Y-axis, pitching moment can be modelled as:

$$\tau_y = T_f \sin\beta \cdot x, \dots (4)$$

where β is the angle made by the other pair of fins. **Note:** for simplicity and understanding of the reader, we consider that only one pair of fins is actuated at a time.

5.5 Yawing

The yaw motion on the UAV is controlled with respect to the difference in angular speeds of the two rotors: ω_1 and ω_2 . As these rotors rotate in opposing directions, their resultant torques are nullified by each other. From Newton's second law, the resultant yaw moment can be described as:

$$\tau_z = I_{zz} (\omega_1 - \omega_2)$$

$$\tau_z = I_{zz} (\Delta\omega)$$

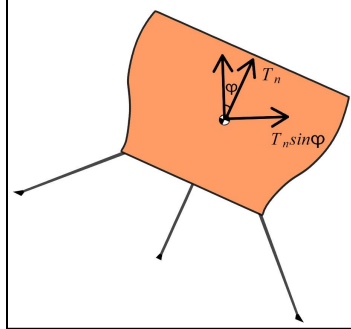
$$\tau_z = \frac{1}{2} I_{zz1} \Delta\omega_1 + \frac{1}{2} I_{zz2} \Delta\omega_2 \dots (5)$$

where I_{zz} is the moment of inertia of the CCW propeller about the Z-axis and I_{zz2} is the moment of inertia of the CW propeller.

5.6 Horizontal Motion

The equations of horizontal motion can be derived from the Newton-Euler concept. Let's consider ϕ, θ, ψ as the Euler angles for roll, pitch and yaw respectively. Assuming that the UAV rolls for an angle ϕ when a rolling moment τ_x is applied, the horizontal motion along the X-axis can be described as:

$$x'' = \frac{-T_n \sin\phi}{m} \dots (6)$$



Similarly, horizontal motion along the Y-axis can be described as:

$$y'' = \frac{T_n \sin\theta}{m} \dots (7)$$

5.7 Control Vector

Now, we can compute all the angular speeds of the rotors and the angle of the fins based on the control vector $U = [T \tau_x \tau_y \tau_z]^T$ in the inertial frame of reference using the following matrix equation:

$$\begin{bmatrix} T \\ \tau_x \\ \tau_y \\ \tau_z \end{bmatrix} = \begin{bmatrix} K_T & K_T & 0 & 0 & 0 & 0 \\ 0 & 0 & xT_{f1} & 0 & 0 & 0 \\ 0 & 0 & 0 & xT_{f2} & 0 & 0 \\ 0 & 0 & 0 & 0 & I_{zz1} & I_{zz2} \end{bmatrix} \begin{bmatrix} \omega_1^2 \\ \omega_2^2 \\ \sin\alpha \\ \sin\beta \\ \frac{\Delta\omega_1}{2} \\ \frac{\Delta\omega_2}{2} \end{bmatrix} \dots (8)$$

5.8 State-Space Representation

A state-space representation is a mathematical model described by first-order differential equations consisting of a set of input, output and state variables of any arbitrary system. State variables with representing axes are collectively termed as *State-Space* [24]. Generally, the state-space representation of a linear system can be described with the following two equations:

$$\dot{x}(t) = Ax(t) + Bu(t) \dots (9)$$

$$y(t) = Cx(t) + Du(t) \dots (10)$$

where, $x(t)$ is the state vector; $y(t)$ is the output vector; $u(t) = [T \tau_x \tau_y \tau_z]^T$ is the input/control vector; A is the system matrix; B is the input matrix; C is the output matrix; D is the feed-forward matrix. Here $x(t) = [x \dot{x} \ddot{x} y \dot{y} \ddot{y} z \dot{z} \ddot{z} \phi \dot{\phi} \ddot{\phi} \theta \dot{\theta} \ddot{\theta} \psi \dot{\psi} \ddot{\psi}]$ is the state vector where $x, y, z, \dot{x}, \dot{y}, \dot{z}$ denote position in cartesian space and their derivatives; and $\phi, \dot{\phi}, \ddot{\phi}, \theta, \dot{\theta}, \ddot{\theta}, \psi, \dot{\psi}, \ddot{\psi}$ denote 3D orientation and their respective angular rates.

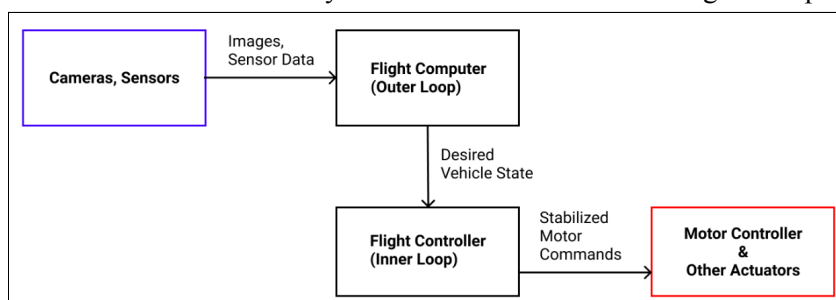
From equation (9), the state-space representation of the system can be formulated as:

$$\begin{array}{c} x(t) \\ \hline \begin{bmatrix} x \\ \dot{x} \\ \ddot{x} \\ y \\ \dot{y} \\ \ddot{y} \\ z \\ \dot{z} \\ \ddot{z} \\ \phi \\ \dot{\phi} \\ \ddot{\phi} \\ \theta \\ \dot{\theta} \\ \ddot{\theta} \\ \psi \\ \dot{\psi} \\ \ddot{\psi} \end{bmatrix} \end{array} = \begin{array}{c} A \\ \hline \begin{bmatrix} 0 & 0 & 0 & 1 & 0 & 0 & 0 & 0 & 0 & 0 & 0 & 0 & 0 & 0 & 0 & 0 \\ 0 & 0 & 0 & 0 & 1 & 0 & 0 & 0 & 0 & 0 & 0 & 0 & 0 & 0 & 0 & 0 \\ 0 & 0 & 0 & 0 & 0 & 1 & 0 & 0 & 0 & 0 & 0 & 0 & 0 & 0 & 0 & 0 \\ 0 & 0 & 0 & 0 & 0 & 0 & 0 & -\frac{T_n}{m} & 0 & 0 & 0 & 0 & 0 & 0 & 0 & 0 \\ 0 & 0 & 0 & 0 & 0 & 0 & 0 & 0 & \frac{T_n}{m} & 0 & 0 & 0 & 0 & 0 & 0 & 0 \\ 0 & 0 & 0 & 0 & 0 & 0 & 0 & 0 & 0 & \frac{T_n}{m} & 0 & 0 & 0 & 0 & 0 & 0 \\ 0 & 0 & 0 & 0 & 0 & 0 & 0 & 0 & 0 & 0 & 0 & 0 & 0 & 0 & 0 & 0 \\ 0 & 0 & 0 & 0 & 0 & 0 & 0 & 0 & 0 & 0 & 0 & 0 & 0 & 0 & 0 & 0 \\ 0 & 0 & 0 & 0 & 0 & 0 & 0 & 0 & 0 & 0 & 0 & 0 & 0 & 0 & 0 & 0 \\ 0 & 0 & 0 & 0 & 0 & 0 & 0 & 0 & 0 & 0 & 0 & 0 & 0 & 0 & 0 & 0 \\ 0 & 0 & 0 & 0 & 0 & 0 & 0 & 0 & 0 & 0 & 0 & 0 & 0 & 0 & 0 & 0 \\ 0 & 0 & 0 & 0 & 0 & 0 & 0 & 0 & 0 & 0 & 0 & 0 & 0 & 0 & 0 & 0 \\ 0 & 0 & 0 & 0 & 0 & 0 & 0 & 0 & 0 & 0 & 0 & 0 & 0 & 0 & 0 & 0 \\ 0 & 0 & 0 & 0 & 0 & 0 & 0 & 0 & 0 & 0 & 0 & 0 & 0 & 0 & 0 & 0 \\ 0 & 0 & 0 & 0 & 0 & 0 & 0 & 0 & 0 & 0 & 0 & 0 & 0 & 0 & 0 & 0 \\ 0 & 0 & 0 & 0 & 0 & 0 & 0 & 0 & 0 & 0 & 0 & 0 & 0 & 0 & 0 & 0 \\ 0 & 0 & 0 & 0 & 0 & 0 & 0 & 0 & 0 & 0 & 0 & 0 & 0 & 0 & 0 & 0 \end{bmatrix} \end{array} \begin{array}{c} x(t) \\ \hline \begin{bmatrix} x \\ \dot{x} \\ \ddot{x} \\ y \\ \dot{y} \\ \ddot{y} \\ z \\ \dot{z} \\ \ddot{z} \\ \phi \\ \dot{\phi} \\ \ddot{\phi} \\ \theta \\ \dot{\theta} \\ \ddot{\theta} \\ \psi \\ \dot{\psi} \\ \ddot{\psi} \end{bmatrix} \end{array} + \begin{array}{c} B \\ \hline \begin{bmatrix} 0 & 0 & 0 & 0 \\ 0 & 0 & 0 & 0 \\ 0 & 0 & 0 & 0 \\ 0 & 0 & 0 & 0 \\ 1 & \frac{1}{m} & 0 & 0 & 0 \\ 0 & 0 & 0 & 0 & 0 \\ 0 & 0 & 0 & 0 & 0 \\ 0 & 0 & 0 & 0 & 0 \\ 0 & 0 & 0 & 0 & 0 \\ 0 & 0 & 0 & 0 & 0 \\ 0 & 0 & 0 & 0 & 0 \\ 0 & 0 & 0 & 0 & 0 \\ 0 & 0 & 0 & 0 & 0 \\ 0 & 0 & 0 & 0 & 0 \\ 0 & 0 & 0 & 0 & 0 \\ 0 & 0 & 0 & 0 & 0 \end{bmatrix} \end{array} \begin{array}{c} u(t) \\ \hline \begin{bmatrix} T \\ \tau_x \\ \tau_y \\ \tau_z \end{bmatrix} \end{array} \dots(11)$$

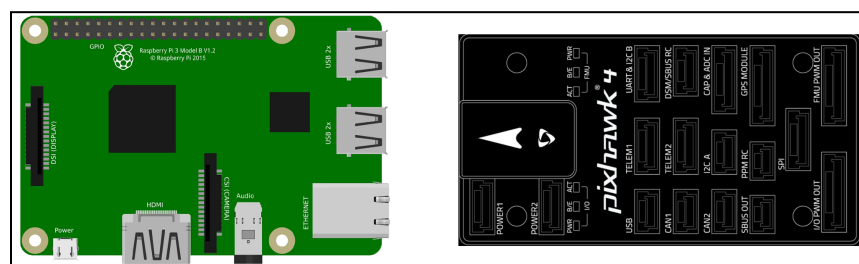
Thus, equation (11) defines the 6-DOF state-space of the UAV's dynamic system.

6. UAV Flight System Control

In order to obtain a certain level of autonomy in the mobility of the UAV, there are two levels of control that need to be achieved. The first level is the *Inner Loop Control* (ILC). This controller stabilizes the flight of the UAV and keeps the UAV at a desired attitude and body rate. The second level is the *Outer Loop Control* (OLC). This controller generates desired position, angle and rate commands to move the UAV from point A to B. The ILC is the responsibility of an integral component called the Flight Controller. While the OLC is taken care of by an onboard CPU called the Flight Computer.

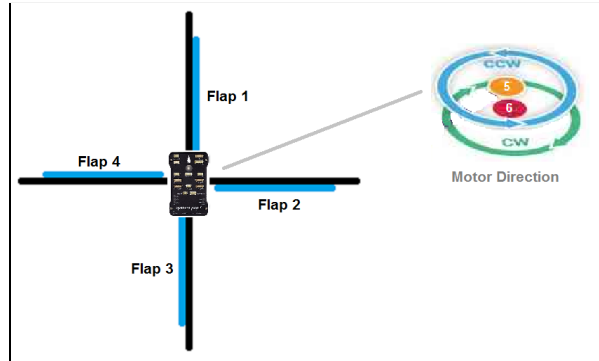


6.1 Flight Controller and Flight Computer Interface



For our UAV we will be using Raspberry Pi 4 (RPi) as the Flight Computer and Pixhawk 4 as the Flight Controller.

The RPi runs Ubuntu Mate OS while the Pixhawk 4 runs the open-source ArduPilot Firmware. For our purpose, we will use ArduPilot CoaxCopter [25]. The Coaxial Rotor configuration is illustrated in the following figure.



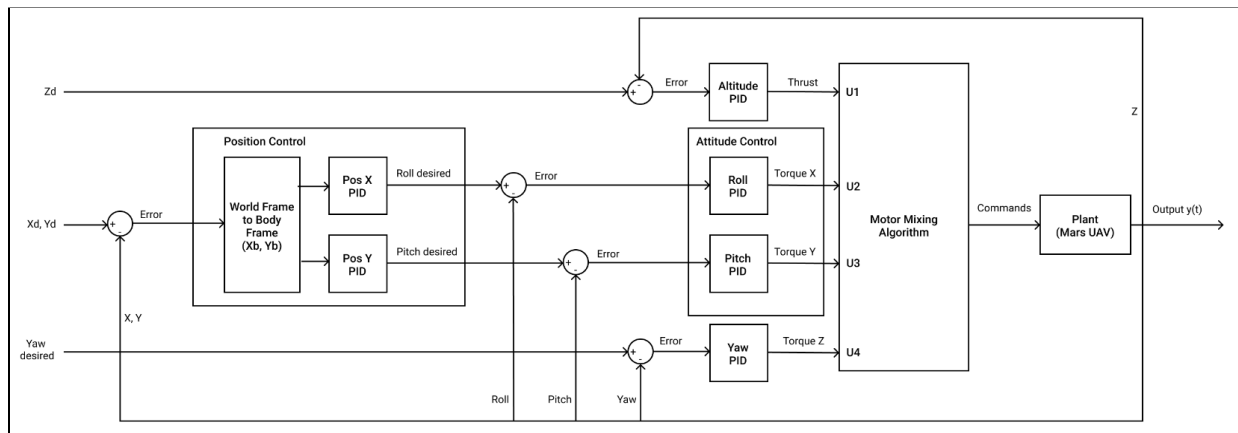
The documentation and instructions for loading the firmware are mentioned in [25]. Once the UART Serial Port has been enabled on RPi and things have been set up, we can proceed to create an interface between RPi and Pixhawk 4.

6.1.1 MAVLink Protocol & DroneKit

The MAVLink protocol enables RPi and Pixhawk to exchange data via serial communication. [26] shows how to establish communication between RPi and Pixhawk via MAVLink. Furthermore, MAVProxy is a command-line tool that enables RPi to send commands via terminal. In contrast, DroneKit-Python is a library that enables RPi x Pixhawk communication via actual Python scripting [27]. For our purpose, we will be using the DroneKit-Python library in ROS Nodes to perform autonomous tasks.

6.2 Closed-Loop Control

In this section, the Inner Loop Control performed by Pixhawk 4 is explained. In our UAV's control algorithm, we will be using closed-loop PID controllers for Altitude, Attitude, Heading and Position control.



The control diagram above illustrates a Closed-Loop control system for our UAV.

6.2.1 Altitude PID Control

The Altitude PID controller is responsible for producing the thrust control signal, U_1 .

Mathematically, it can be expressed as:

$$U_1 = k_p(z_d - z) + k_d(\dot{z}_d - \dot{z}) + k_i \int (z_d - z) dt + mg \dots (1)$$

Where k_p is the proportional gain; k_d is the derivative gain; k_i is the integral gain. Similarly, Roll, Pitch, Yaw and Position PID controllers can be expressed in the same manner. All PID controllers are pre-tuned in the ArduPilot Firmware.

6.2.2 Motor Mixing Algorithm (MMA)

The motor mixing algorithm computes the angular speeds the rotors are required to rotate at. It also computes the servo angle of fins for direction control. From equation (8) in section 7: *Flight Dynamics*, the MMA can obtain values of ω_1 , ω_2 , α , β , $\Delta\omega_1$, $\Delta\omega_2$ (α , β are servo angle) using the equations given below:

$$\omega_{cw} = \omega_1 + 0.5\Delta\omega_1 \dots (2) \quad \omega_{ccw} = \omega_2 - 0.5\Delta\omega_2 \dots (3) \quad \alpha = \sin^{-1}\left(\frac{\tau_x}{T_f \cdot x}\right) \dots (4)$$

$$\beta = \sin^{-1}\left(\frac{\tau_y}{T_f \cdot y}\right) \dots (5)$$

7. Reconnaissance Mission

The UAV must be capable of capturing a digital orthophoto of a patch of land on Mars measuring at least 300 square meters. An orthophoto is an aerial photograph that has been geometrically corrected or ortho-rectified such that the scale of the photograph is uniform and utilised in the same manner as a map [28]. Now, we shall first consider the requirements to generate an orthophoto. The requirements are listed out as follows:

1. Aerial Image/s of the surface of interest.
2. Digital Terrain Model of the surface of interest.
3. Real-time localisation and odometry information.

7.1 Aerial Imagery

In order to perform ortho-rectification, the UAV will require a high-resolution aerial camera (one which is not too heavy because of the lens's weight and one which is compatible with RPi). For our needs, we will be using the Raspberry Pi HQ Camera, equipped with a 6 mm CS Mount Wide-Angle Lens. The CS-mount lens is highly suitable for distance and telephotography. The technical specifications of the Lens can be found here [29].

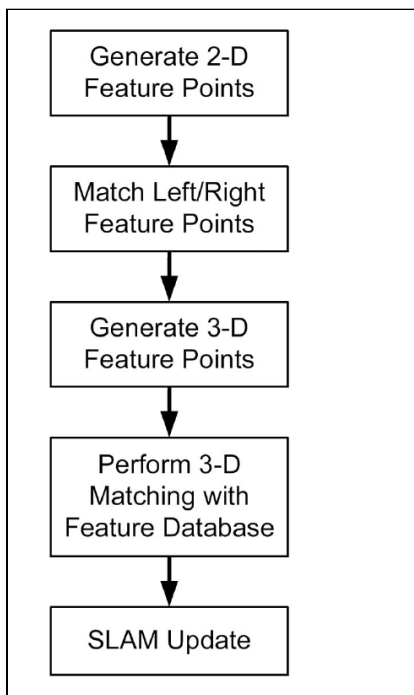


(a) RPi HQ Camera; (b) CS-mount Lens; (c) UAV mounting and setup.

7.2 Digital Terrain Model

To ortho-rectify images, the height information of every point in the terrain/surface is required. Without this information, ortho-rectification is not possible. There are two ways of obtaining the height information.

1. The first one is to use an existing Digital Terrain Model (DTM) of the surface of interest. We can use DTMs captured by the HiRISE camera on the MRO. A database of DTMs captured by HiRISE can be found in [30]. DTMs of specific locations in Mars can be downloaded and stored in the external memory of RPi thereby allowing the UAV to create orthophotos of that specific location.
2. The second way of obtaining the height information for the surface of interest would be to perform dense 3D reconstruction using bundle-adjustment optimization and keyframe based stereo vision approach.

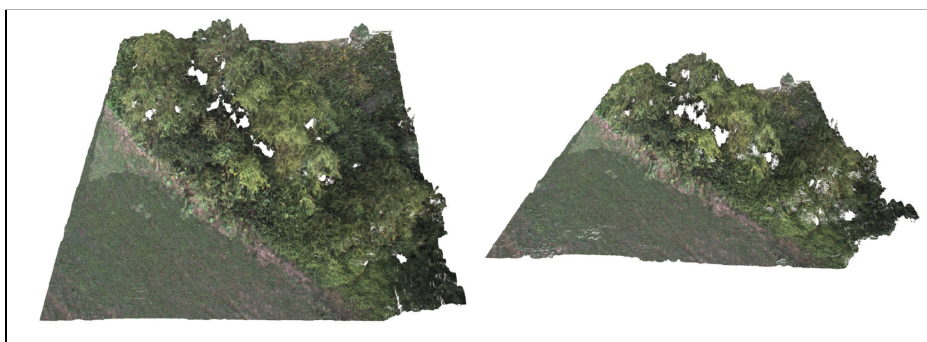


The algorithm proposed in [31] incorporates the use of a wide-baseline stereo camera for real-time rapid terrain mapping.
 Thus, for our UAV, we designed a wide-baseline stereo camera setup

Block diagram (left) courtesy - [31]

Algorithm: Terrain Mapping
 for each frame

- | Rectify the left and right images based on the stereo calibration.
- | Generate feature points from the stereo image pair
- | for every left feature point
 - | search along the epipolar line in the right image for the nearest-neighbour match
 - | Project the match to a 3-D coordinate relative to the camera.
 - | Store the 3-D coordinate for each match.
 - | Perform matching with previous frames.
 - | Reduce match error using IMU data.
 - | Update 3D Terrain Map using SLAM.



Digitally mapped terrain of tree farm from an altitude of 40 m. The minimum cumulative spatial error is 1.7%. Courtesy - [31]

7.3 Generating an Orthophoto

The basic algorithm of creating an orthophoto is explained.

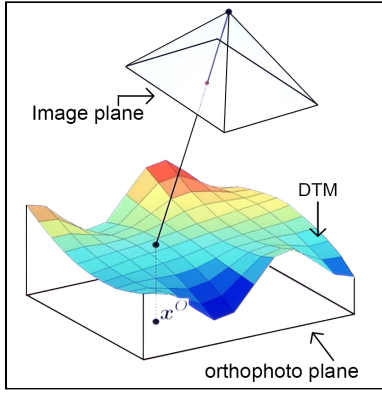


Image (left) Courtesy - Schindler

Algorithm: Generating Orthophoto

for each aerial image

- | Take a point on the orthophoto-plane x^o
- | Determine the surface point $X = [x \ y \ z]^T$ from x^o
- | Map the surface point to the image plane: $x^k = PX$
- | Copy the image intensity value of x^k to x^o : $I(x^k) = I(x^o)$
- | Repeat the above 4 steps for every point on the orthophoto plane.

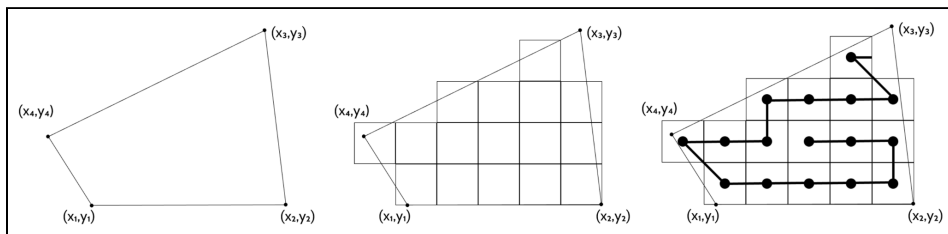
Note: we perform bilinear and bicubic interpolation for the latter and former respectively.

7.4 UAV Waypoint Trajectory for Orthophoto Generation

The UAV uses Visual-Inertial Odometry (VIO) to estimate position (Long. & Lat.) and attitude during flight as proposed by the authors of [32]. A ROS package for VIO can be found in [33]. The first step of generating orthophotos is to take proper aerial photographs of the surface of interest. The UAV is made to fly at ~ 122.4 m altitude to cover a sufficient area of land (~ 150 m 2). Let's consider that the UAV has to generate a digital orthophoto of a patch of land linearly enclosed by four points as shown in figure below. We propose the following algorithm to tackle this problem.

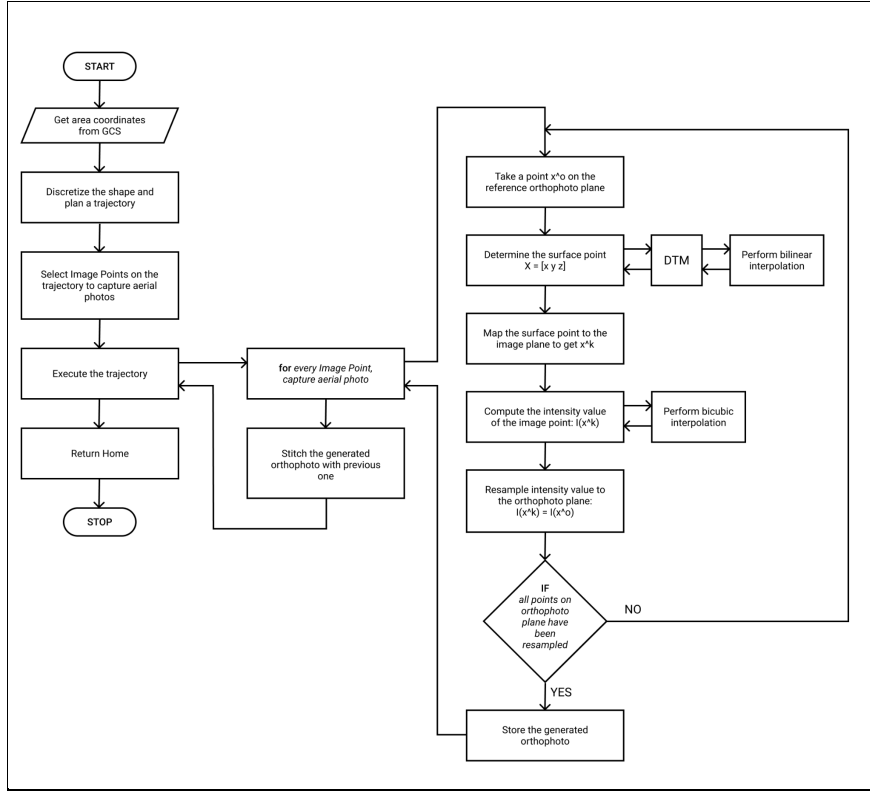
Algorithm: Aerial Imaging and Trajectory Computation

- | Get the 4 coordinates of the surface of interest: $P = [x_1 \ y_1; x_2 \ y_2; x_3 \ y_3; x_4 \ y_4]$.
- | Discretize the quadrilateral shape of the land area into smaller squares of size 150 square meters.
- | Compute the shortest trajectory covering each square.
- | Select points on the trajectory where aerial images must be captured.
- | Execute the trajectory (using VIO algorithm [32] for pose estimation) from the desired altitude.
- | Take aerial photographs from select points.
- | Return home.



(Left) shows a patch of land enclosed by 4 coordinates which are to be converted into an orthophoto; (Center) illustrates discretization which is step 2 of the algorithm; (right) illustrates trajectory computation and image point selection which steps 3 and 4 respectively.

7.5 Putting It All Together: Final Algorithm



8. Logistics Mission

8.1 Mechanical Setup

A simple mechanism has been designed in order to carry out this task. The frame of the UAV has a ‘H-shaped’ slot (Fig. 8.1) built into it. Under the ‘H-shaped’ slot, there are sliders. These sliders are moved with the help of a servo motor. The servo motor is connected to a crankshaft, which is in turn connected to a connecting rod. This rod connects both the sliders. The figure 8.2 shows the highlighted sliders.

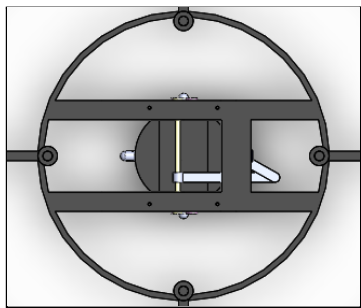


Fig. 8. 1

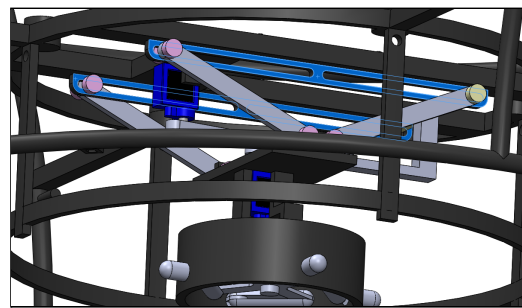


Fig. 8. 2

Fig. 8.2 shows that, when the sliders are at the extreme ends, the ‘payload holder’ is raised. The ‘payload holder’ is highlighted in fig 8.3. The position of the sliders and the height of the payload holder depend on the angle of the crank as shown in figures [8.4] & [8.5].

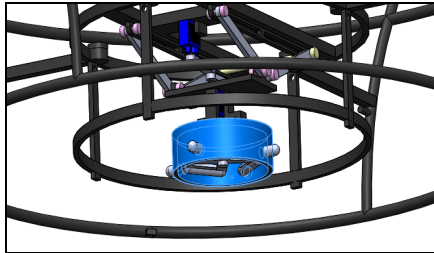


Fig. 8.3

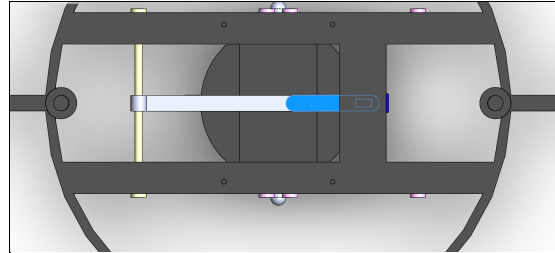


Fig. 8.4

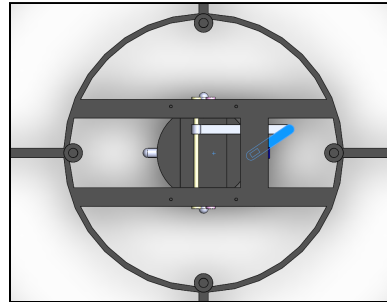


Fig. 8.5

As the ‘payload holder’ is lowered, the pins on the holder are retracted by another servo motor. The holder is made to go into an opening that is on the payload. When the holder is in the payload, the pins of the holder are moved outward with the help of the servo motor. This helps the holder attach to the payload. Fig. [8.6] shows the highlighted pins. Fig. [8.7] shows the mechanism used to retract and push the pins. The servo motor rotates the shaft anti clockwise, which inturn retracts the pins. It is easily repairable.

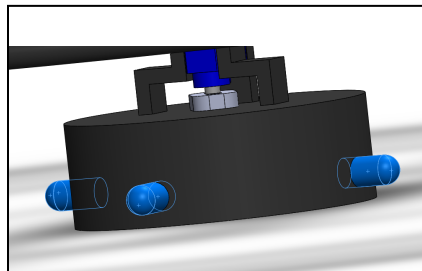


Fig. 8.6

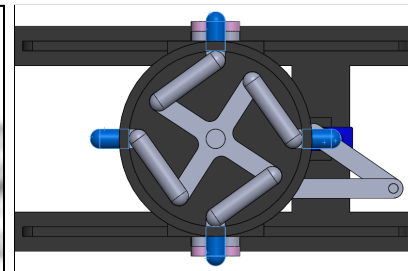


Fig. 8.7

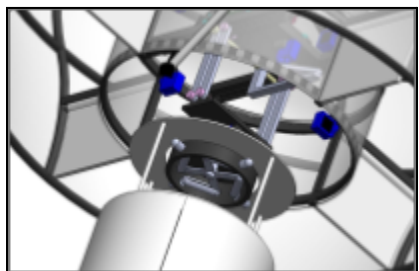


Fig. 8.8

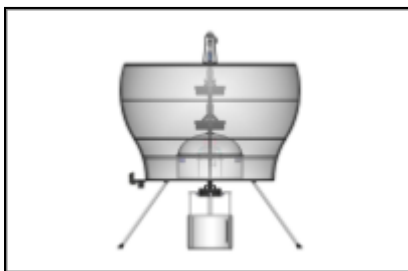


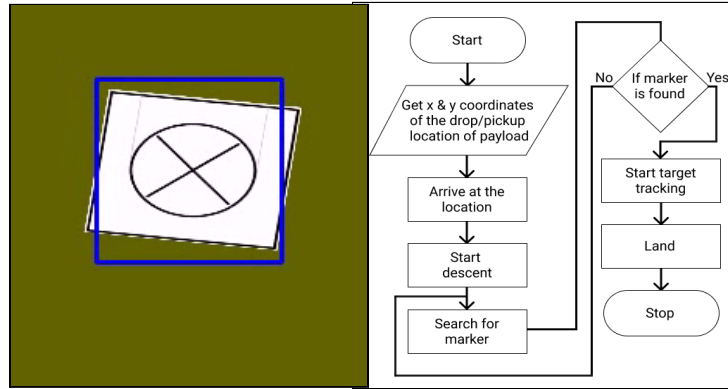
Fig. 8.9

10.2 Autonomous Precision Landing

Precision landing is required in order for the UAV to autonomously pick up and drop payload packages at desired locations. In order to accomplish this, we intend to use the GitHub Repository [nikv96/AutonomousPrecisionLanding](https://github.com/nikv96/AutonomousPrecisionLanding) [34]. The prerequisites for using the repository are: (i) MavProxy

(ii) Dronekit. Both the dependencies have been satisfied (as discussed in section: *UAV System Control*). The project utilizes the dronekit-python library to connect to a Pixhawk flight controller [34]. The target tracking is performed using Viola Jones approach of Rapid Object Detection using HAAR-cascades [35]. A marker can be attached to the upper surface of the payload in order for the UAV to track it and perform precision landing. The figure below (on the left) shows target tracking performed in a simulated environment using

Dronekit-sitl [34].



9. Atmospheric Analysis Mission

The martian atmosphere is composed of 95% by volume of carbon dioxide (CO₂), 2.6% molecular nitrogen (N₂), 1.9% argon (Ar), 0.16% molecular oxygen (O₂), and 0.06% carbon monoxide (CO) [36]. In this section, we shall discuss how the UAV analyses the martian atmosphere.

9.1. Temperature and Humidity Sensing

For measuring the temperature and humidity on mars, we use the DHT22 sensor. The sensor has high accuracy, resolution and a wide measuring range.

Powers supply	3.3 - 6 Volts	
Output signal	Single-bus signal	
Sensing element	Polymer capacitor	
Operating range	Relative humidity: 0 to 100%	Temperature: -50 to 80°C
Accuracy	Relative humidity: ± 2%	Temperature: ±0.5°C
Resolution	Relative humidity: 0.1%	Temperature: 0.1°C



Note: The average temperature of mars is -63°C which is lesser than the minimum operating temperature of DHT22. Since the UAV is set to fly during the day (~11 AM Mars Time), the atmospheric temperature rises to much higher values than -63°C and remains well within the operating range of the sensor.

9.2 Carbon Dioxide (CO₂) Sensing

Carbon Dioxide is the most abundant gas in the martian atmosphere. Based on our research, a Nondispersive Infrared (NDIR) sensor was the apt choice for measuring CO₂ content in air. NDIR sensors work based on Infrared Optics where the attenuation of wavelengths can be studied to predict the presence and composition of a gas, in our case CO₂ [37]. For our application, we will be using the SprintIR6S NDIR CO₂ sensor [38].

Power supply	3.3V recommended
Temperature Range	-30°C to +70°C
Measurement Range	0-100%
Accuracy	±70 ppm
Peak and average current	33mA and 12mA



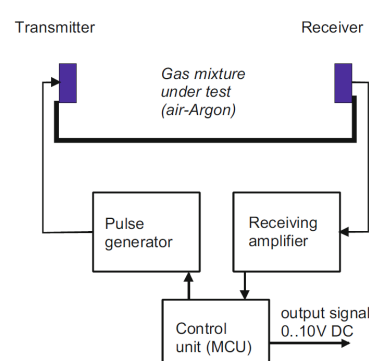
9.3 Argon Gas Detection

Argon constitutes only about 1.9% of Mars's atmosphere. In order to determine the argon content in the air, we employ an acoustic method. In this method, we measure the speed of sound. This can be useful for determining argon content in an argon-air mixture because the speed of sound varies as the argon-air ratio changes [39].

In earth conditions, the speed of sound changes from 343 m/s to 319 m/s as the argon-air ratio changes from 0 to 1 [39]. Using this property, an ultrasonic transmitter and receiver can be used to determine the speed of sound if the distance between them is known. We use a modified version of the HC-SR04 ultrasonic range sensor where the transmitter and receiver are kept facing each other and separated by a distance of 150 mm. With time and distance known, we can calculate the speed of sound using the following equation:

$$\text{speed} = \frac{\text{distance}}{\text{time}}$$

HC-SR04 Specifications [40]	
Power supply	5 Volts
Working current	15mA
Working Frequency	40 Hz
Propagation angle	15° degrees
Type	Ultrasonic



9.4 Oxygen (O₂) sensing

We use the Grove - Oxygen Sensor [41] to determine the oxygen concentration in air. This sensor works on the principle of an electrochemical cell. The output current from the sensor varies according to

the concentration of oxygen in the air and the same can be determined by comparing the current to the characteristic graph of the sensor which can be found in [41].

Input Voltage	3.3V / 5V
Detect Life	2 years
Sensitivity	0.05~0.15 mA
Temperature Range	-20°C to +50°C
Measurement Range	0% to 25%



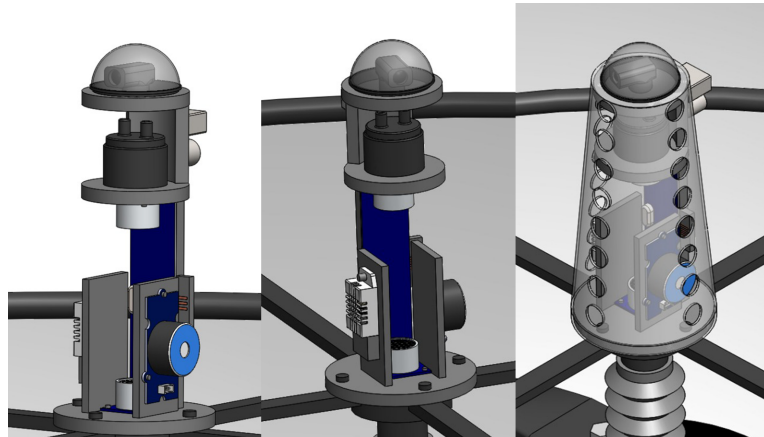
9.5 Nitrogen (N_2) estimation

As per our survey and research, there was no lightweight sensor that was capable of operating in low-temperature martian conditions. Therefore, we use the following equation to estimate the percentage of nitrogen in the atmosphere:

$$\%N_2 = 100 - (\%CO_2 + \%Ar + \%O_2)$$

This estimation can still yield an accurate value. **Note:** Since carbon monoxide constitutes an extremely low percentage of Mars's atmosphere, we neglect its presence.

9.6 Atmospheric Analysis Module Setup



References:

1. "Mars Fact Sheet," <https://nssdc.gsfc.nasa.gov/planetary/factsheet/marsfact.html>
2. Akash Patel, "Design, Modelling and Control of a Space UAV for Mars Exploration," *Space Engineering, master's level*, 2021
3. <https://www.nasa.gov/feature/goddard/2019/with-mars-methane-mystery-unsolved-curiosity-serv es-scientists-a-new-one-oxygen>
4. <https://airandspace.si.edu/exhibitions/exploring-the-planets/online/solar-system/mars/wind/#:~:text=Because%20the%20atmosphere%20is%20so,per%20hour%20during%20dust%20storms.>
5. https://en.wikipedia.org/wiki/Atmosphere_of_Mars
6. <https://mars.nasa.gov/mars2020/participate/sounds/#:~:text=With%20an%20average%20surface%20temperature,meters%20per%20second>
7. https://en.wikipedia.org/wiki/Flow_separation#:~:text=Flow%20separation%20or%20boundary%20layer,a%20widening%20passage%2C%20for%20example.
8. Snorri Gudmundsson, "General Aviation Aircraft Design, Applied Methods and Procedures; Chapter 14: The Anatomy of the Propeller," 2013
9. <https://www.grc.nasa.gov/www/k-12/airplane/proph.html>
10. E Natarajan, "Engineering Thermodynamics: Fundamentals and Applications" *Anuragam Publications*, 2014
11. <https://www.mars-one.com/faq/mission-to-mars/what-are-the-risks-of-dust-and-sand-on-mars>
12. Stefano Gaggero, Diego Villa, Giorgio Tani, Michele Viviani, Daniele Bertetta, "Design of ducted propeller nozzles through a RANSE-based optimization approach" *Ocean Engineering, ELSEVIER*, 2017
13. <http://gemsmotor.com/12v-24v-48v-brushless-blcd-motor>
14. Lithium-ion Power System for Small Satellites -
(<https://www.jpl.nasa.gov/nmp/st5/TECHNOLOGY/battery.html#:~:text=And%2C%20they%20need%20to%20work,space%20flight%20are%20nickel%2Dcadmium.>)
15. Ratnakumar Bugga, Marshall Smart, Jay Whitacre, William West, Lithium-Ion Batteries for Space Applications" *IEEE Aerospace Conference*, 2007
16. Lithium polymer battery, Wikipedia - (https://en.wikipedia.org/wiki/Lithium_polymer_battery)
17. <https://www.exploreenergies.com/electric-vehicle-lifepo4-battery-pack.html>
18. T300 Data Sheet - T300DataSheet_1.pdf (rockwestcomposites.com)
19. AA7075 T7351 - [7075 Aluminum: Get to Know its Properties and Uses - Gabrian](#)
20. PTFE characteristics -
<https://omnexus.specialchem.com/selection-guide/polytetrafluoroethylene-ptfe-fluoropolymer>
21. Carbon Fibre properties -
<https://www.toraycma.com/wp-content/uploads/M40J-Technical-Data-Sheet-1.pdf.pdf>
22. Wang, Miao, Feng, Junzong, "Preparation and properties of the multi-layer aerogel thermal insulation composites," 2018
23. <https://gmnameplate.com/company/blog/what-are-ptc-heaters>
24. Z. Tahir, W. Tahir and S. A. Liaqat, "State-space system Modeling of a Quadcopter UAV," arXiv preprint arXiv:1908.07401, 2019
25. <https://ardupilot.org/copter/docs/singlecopter-and-coaxcopter.html>
26. <https://ardupilot.org/dev/docs/raspberry-pi-via-mavlink.html#communicating-with-raspberry-pi-v ia-mavlink>

27. <https://dronekit-python.readthedocs.io/en/latest/>
28. <http://www.photomapping.com.au/digital-orthophoto#:~:text=An%20orthophoto%20is%20an%20aerial,of%20features%20within%20the%20photograph.>
29. 6mm CS-mount Wide Angle Lens Datasheet
30. HiRISE DTM Catalog - (<https://www.uahirise.org//dtm/>)
31. Kevin V. Stefanik, Jason C. Gassaway, Kevin Kochersberger, A. Lynn Abbott, “UAV-Based Stereo Vision for Rapid Aerial Terrain Mapping” *GIScience & Remote Sensing*, 2011
32. Davide Scaramuzza, Zichao Zhang, “Visual-Inertial Odometry of Aerial Robots” *arXiv:1906.03289v2 [cs.RO]*, 2019
33. VIODOM ROS package - (<https://github.com/fjperezgrau/viodom>)
34. AutonomousPrecisionLanding - (<https://github.com/nikv96/AutonomousPrecisionLanding>)
35. Paul Viola, Michael Jones, “Rapid Object Detection using a Boosted Cascade of Simple Features,” *Conference on Computer Vision and Pattern Recognition*, 2001
36. With Mars Methane Mystery Unsolved, Curiosity Serves Scientists a New One: Oxygen - (<https://www.nasa.gov/feature/goddard/2019/with-mars-methane-mystery-unsolved-curiosity-serves-scientists-a-new-one-oxygen>)
37. Nondispersive infrared sensor - (https://en.wikipedia.org/wiki/Nondispersive_infrared_sensor)
38. SprintIR6S NDIR CO₂ sensor - (<https://projects-raspberry.com/sprintir6s-worlds-fastest-ndir-co2-sensor/>)
39. Artur Jedrusyna, Andrzej Noga, “Acoustic detector of argon content in air-argon mixture” *Advances in Intelligent Systems and Computing, Springer International Publishing Switzerland*, 2016
40. HC-SR04 datasheet (<https://cdn.sparkfun.com/datasheets/Sensors/Proximity/HCSR04.pdf>)
41. Grove Oxygen Sensor (https://wiki.seeedstudio.com/Grove-Gas_Sensor-O2/)

Team Members

Punitharaj S, Shimon Thomas Sajan, Purveen Ram, Mohammad Hamdaan,
Pranavan S, Sneha B, Jaba Raja Simona M, J Johanan Sherwyn, Sakthivel,
Alfred Jerome G, Lokeshwaran E, Praveen E

Acknowledgement

We give thanks to
the HODs:
Dr Queen Florence Mary (Mechanical)
Dr Prathiba S (EEE)
Dr Egfin Nirmala D (ECE)
and
the management of
Loyola-ICAM College of Engineering and Technology.

Special mention to
Prof. Prabhu Shankar, Prof. Ramya Hyacinth, Prof. James Deepak D
for being supportive and helpful.